Biophysical Journal, Volume *121*

Supplemental information

Interplay between Brownian motion and cross-linking controls bundling dynamics in actin networks

Ondrej Maxian, Aleksandar Donev, and Alex Mogilner

Supplemental text

Interplay between Brownian motion and cross-linking kinetics controls bundling dynamics in actin networks

Ondrej Maxian, Aleksandar Donev, and Alex Mogilner

A Rigid fibers as a special case of inextensible fibers

In [S1], we discretized the inextensible system Eq. (2) (equation numbers refer to the article main text) by discretizing each fiber with N Chebyshev collocation points and representing the functions $\alpha_1(s)$ and $\alpha_2(s)$ by their Chebyshev coefficients, $\alpha_j(s) = \sum_{k=0}^{N-2} \alpha_{jk} T_k(s)$. Our goal here is to show that setting $\alpha_j(s) = \alpha_j = \text{const.}$ instead gives the straight rigid fiber kinematic operators Eqs. (8) and (9). For convenience, we first restate the kinematic equations for inextensible fibers, which are Equations (41) and (44) in [S1],

$$(\boldsymbol{\mathcal{K}}[\boldsymbol{X}]\boldsymbol{\alpha})(s) = \overline{\boldsymbol{U}} + \int_0^s \sum_{j=1}^{2} \sum_k \alpha_{jk} T_k\left(s'\right) \boldsymbol{n}_j\left(\boldsymbol{\tau}(s')\right)\, ds' \tag{S1}$$

$$\boldsymbol{\mathcal{K}}^*[\boldsymbol{X}]\boldsymbol{\lambda} := \begin{pmatrix} \int_0^L \left(\int_0^s T_k(s') \boldsymbol{n}_1\left(\boldsymbol{\tau}(s')\right)\, ds'\right) \cdot \boldsymbol{\lambda}(s)\, ds \\ \int_0^L \left(\int_0^s T_k(s') \boldsymbol{n}_2\left(\boldsymbol{\tau}(s')\right)\, ds'\right) \cdot \boldsymbol{\lambda}(s)\, ds \\ \int_0^L \boldsymbol{\lambda}(s)\, ds \end{pmatrix} = \begin{pmatrix} 0 \\ 0 \\ \boldsymbol{0} \end{pmatrix}, \tag{S2}$$

where the first two components of (S2) hold for all k. Let us denote by $\boldsymbol{\mathcal{K}}_s$ the operator $\boldsymbol{\mathcal{K}}$ in the case of straight fibers with $k = 0$ being the only included Chebyshev mode, and likewise for $\boldsymbol{\mathcal{K}}^*$. Then, since the fibers are straight, the orthonormal frame $(\boldsymbol{\tau}, \boldsymbol{n}_1, \boldsymbol{n}_2)$ is constant along the fiber, and thus $\boldsymbol{\mathcal{K}}_s$ and $\boldsymbol{\mathcal{K}}_s^*$ simplify to

$$\boldsymbol{\mathcal{K}}_s\boldsymbol{\alpha} = \overline{\boldsymbol{U}} + \alpha_1 \boldsymbol{n}_1 s + \alpha_2 \boldsymbol{n}_2 s \tag{S3}$$

$$\boldsymbol{\mathcal{K}}_s^*\boldsymbol{\lambda} = \begin{pmatrix} \boldsymbol{n}_1 \cdot \int_0^L s\boldsymbol{\lambda}(s)\, ds \\ \boldsymbol{n}_2 \cdot \int_0^L s\boldsymbol{\lambda}(s)\, ds \\ \int_0^L \boldsymbol{\lambda}(s)\, ds \end{pmatrix}. \tag{S4}$$

We now want to show that $\boldsymbol{\mathcal{K}}_s$ and $\boldsymbol{\mathcal{K}}_r$ (defined in Eq. (8)) parameterize the same linear space of rigid motions. To do this, let us write $\boldsymbol{X}$ in Eq. (8) as an integral of the tangent vector

$$\begin{aligned}
\boldsymbol{\mathcal{K}}_r\boldsymbol{\alpha} &= \boldsymbol{U}_c + \boldsymbol{\Omega}\times(\boldsymbol{X}_0 + s\boldsymbol{\tau} - \boldsymbol{X}_c) && \text{(S5)}\\
&= \boldsymbol{U}_c + \boldsymbol{\Omega}\times(\boldsymbol{X}_0 - \boldsymbol{X}_c) + s\boldsymbol{\Omega}\times\boldsymbol{\tau} && \text{(S6)}\\
&= \widehat{\boldsymbol{U}}_c + s\left((\boldsymbol{\Omega}\cdot\boldsymbol{\tau})\,\boldsymbol{\tau} + (\boldsymbol{\Omega}\cdot\boldsymbol{n}_1)\,\boldsymbol{n}_1 + (\boldsymbol{\Omega}\cdot\boldsymbol{n}_2)\,\boldsymbol{n}_2\right)\times\boldsymbol{\tau} && \text{(S7)}\\
&= \widehat{\boldsymbol{U}}_c + s\left(-(\boldsymbol{\Omega}\cdot\boldsymbol{n}_1)\,\boldsymbol{n}_2 + (\boldsymbol{\Omega}\cdot\boldsymbol{n}_2)\,\boldsymbol{n}_1\right). && \text{(S8)}
\end{aligned}$$

This is exactly the form of $\boldsymbol{\mathcal{K}}_s$ in (S3) with $\alpha_1 = -\boldsymbol{\Omega}\cdot\boldsymbol{n}_2$ and $\alpha_2 = -\boldsymbol{\Omega}\cdot\boldsymbol{n}_1$. So $\boldsymbol{\mathcal{K}}_r$ and $\boldsymbol{\mathcal{K}}_s$ parameterize the same space.

To complete the equivalence, we now show that $\boldsymbol{\mathcal{K}}_s^*\boldsymbol{\lambda} = \boldsymbol{0}$ iff $\boldsymbol{\mathcal{K}}_r^*\boldsymbol{\lambda} = \boldsymbol{0}$. Obviously, $\int_0^L \boldsymbol{\lambda}(s)\,ds = \boldsymbol{0}$ in both cases, so we only have to deal with the torque constraint. If we use the fact that $\int_0^L \boldsymbol{\lambda}(s)\,ds = \boldsymbol{0}$, we can write the second component of Eq. (9) as

$$\begin{aligned}
\boldsymbol{\mathcal{K}}_r^*\boldsymbol{\lambda} &= \int_0^L (\boldsymbol{X}(s) - \boldsymbol{X}_c)\times\boldsymbol{\lambda}(s)\,ds = \int_0^L \boldsymbol{X}(s)\times\boldsymbol{\lambda}(s)\,ds = \int_0^L s\boldsymbol{\tau}\times\boldsymbol{\lambda}(s)\,ds && \text{(S9)}\\
&= \int_0^L s\boldsymbol{\tau}\times\left((\boldsymbol{\tau}\cdot\boldsymbol{\lambda}(s))\,\boldsymbol{\tau} + (\boldsymbol{n}_1\cdot\boldsymbol{\lambda}(s))\,\boldsymbol{n}_1 + (\boldsymbol{n}_2\cdot\boldsymbol{\lambda}(s))\,\boldsymbol{n}_2\right)\,ds && \text{(S10)}\\
&= -\boldsymbol{n}_1\left(\boldsymbol{n}_2\cdot\int_0^L s\boldsymbol{\lambda}(s)\,ds\right) + \boldsymbol{n}_2\left(\boldsymbol{n}_1\cdot\int_0^L s\boldsymbol{\lambda}(s)\,ds\right) && \text{(S11)}
\end{aligned}$$

And now, since $\boldsymbol{n}_1$ and $\boldsymbol{n}_2$ are orthogonal and nonzero, we see from (S4) that $\boldsymbol{\mathcal{K}}_s^*\boldsymbol{\lambda} = \boldsymbol{0} \leftrightarrow \boldsymbol{\mathcal{K}}_r^*\boldsymbol{\lambda} = \boldsymbol{0}$. This shows that we can implement rigid fibers using the same algorithms as in [S1], except we just need to keep a single ($k = 0$) Chebyshev polynomial. Note that the value of κ we use does not matter except for numerical stability since the fibers stay straight for all time, and so we set $\kappa = 0$.

B Form and coefficients of the rigid body mobility matrix

Because of the symmetry of the fiber, the mobility matrix and its "square root" for a single fiber can be written in the form

$$\begin{aligned}
\boldsymbol{N}_{\mathrm{tt}} &= \frac{1}{\mu L}\left(\alpha(\epsilon)\boldsymbol{I} + \beta(\epsilon)\boldsymbol{\tau}\boldsymbol{\tau}\right), \qquad \boldsymbol{N}_{\mathrm{tt}}^{1/2} = \frac{1}{\sqrt{\mu L}}\left(\sqrt{\alpha}\boldsymbol{I} + \left(-\sqrt{\alpha} + \sqrt{\alpha+\beta}\right)\boldsymbol{\tau}\boldsymbol{\tau}\right), && \text{(S12)}\\
\boldsymbol{N}_{\mathrm{rr}} &= \frac{\gamma(\epsilon)}{\mu L^3}\left(\boldsymbol{I} - \boldsymbol{\tau}\boldsymbol{\tau}\right), \qquad \boldsymbol{N}_{\mathrm{rr}}^{1/2} = \sqrt{\frac{\gamma}{\mu L^3}}\left(\boldsymbol{I} - \boldsymbol{\tau}\boldsymbol{\tau}\right).
\end{aligned}$$

Notice that the rotational mobility has a null space of the tangent vector $\boldsymbol{\tau}$. The dimensionless coefficients α, β, and γ are given for various ϵ in Table S1.

ϵ	$\alpha^{(\mathrm{FP})}$	$\beta^{(\mathrm{FP})}$	$\gamma^{(\mathrm{FP})}$
0.01	0.3841	0.2230	3.4263
0.008	0.4020	0.2413	3.6412
0.006	0.4251	0.2646	3.9179
0.005	0.4396	0.2793	4.0931
0.004	0.4575	0.2973	4.3073
0.002	0.5129	0.3530	4.9721
0.001	0.5682	0.4085	5.6361

Table S1: Mobility coefficients for the 6×6 rigid body mobility matrix $\boldsymbol{N}$ defined in (S12) for straight fibers. The numerical estimate of the matrix $\boldsymbol{N}$ is related to the slender body mobility $\boldsymbol{M}$ in Eq. (11), which is computed using intra-fiber hydrodynamics as discussed in the main text section on the mobility.

C Temporal integrator for fluctuating fibers

In this section, we show that our temporal integrator for Brownian motion can accurately reproduce the steady state distribution of link strains. We place two parallel fibers a distance 0.05 apart, so that initially $\boldsymbol{X}^{(1)}(s) = (s, 0, 0)$ and $\boldsymbol{X}^{(2)}(s) = (s, 0.05, 0)$. At $t = 0$, the fibers are connected by a permanent CL attached at the point $s = L = 1$ on each fiber. We use rigid fibers with $N = 50$ points, CL variance $\sigma/L = 0.005$ (to simulate point-force-like springs), spring stiffness $K_c = 10$ pN/μm, and rest length $\ell = 0.05$ μm. We use $\epsilon = 0.004$, $\mu = 0.1$ Pa·s, and $L = 1$ μm, as we do in most of the simulations in the main text. Because we are not interested in dynamics here, we use the local drag mobility, which is Eq. (4) without the integral term. The maximum stable time step is $\Delta t = 0.005$ s, and so we will simulate both with $\Delta t = 0.0005$ s (to get results with small temporal error) and $\Delta t = 0.0025$ s (which is close to the stability limit). We simulate until $t = 100$ seconds in both cases and verify that we run for long enough that we have reached the steady state.

We expect the steady state probability density function (pdf) to be the Gibbs-Boltzmann distribution

$$P(x) = Zx^2 \exp\left(-\frac{K_c(x-\ell)^2}{2kT}\right), \tag{S13}$$

where the constant Z is chosen such that $\int_0^\infty P(x)\,dx = 1$, and the Jacobian x^2 factor is necessary because $P(x)$ is actually the one-dimensional analogue of the true three-dimensional distribution $P(\|\boldsymbol{x}\|)$. Figure S1 (left) shows that the steady state distribution with small Δt agrees with the theory (S13). The right plot, which gives the distributions for Δt =50% of the stability limit, shows

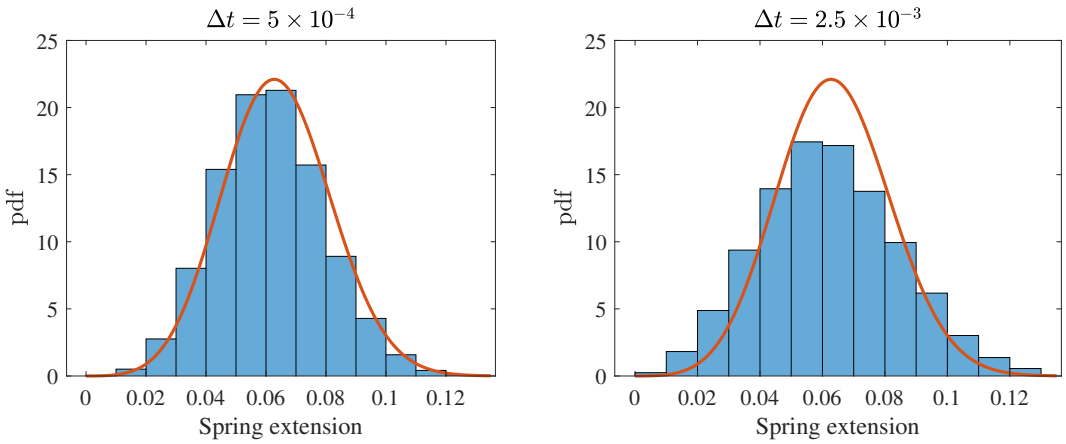

Figure S1: Steady state spring length distribution for two stiff fibers connected by a spring at their endpoint with rest length $\ell = 0.05$ μm. Histograms are the data, and red lines are (S13). Here we use rigid fibers with $N = 50$ points, CL variance $\sigma/L = 0.005$, and spring stiffness $K_c = 10$ pN/μm. We show $\Delta t = 5 \times 10^{-4}$ s =10% of the stability limit on the left, and $\Delta t = 2.5 \times 10^{-3}$ s =50% of the stability limit on the right. The spring extension measurement is performed at the midpoint of the time step (after step 1 in the Temporal Integration section of the main text).

that our temporal integrator can still reproduce the correct distribution with a larger time step size.

References

[S1] Ondrej Maxian, Alex Mogilner, and Aleksandar Donev. Integral-based spectral method for inextensible slender fibers in stokes flow. *Physical Review Fluids*, 6(1):014102, 2021.

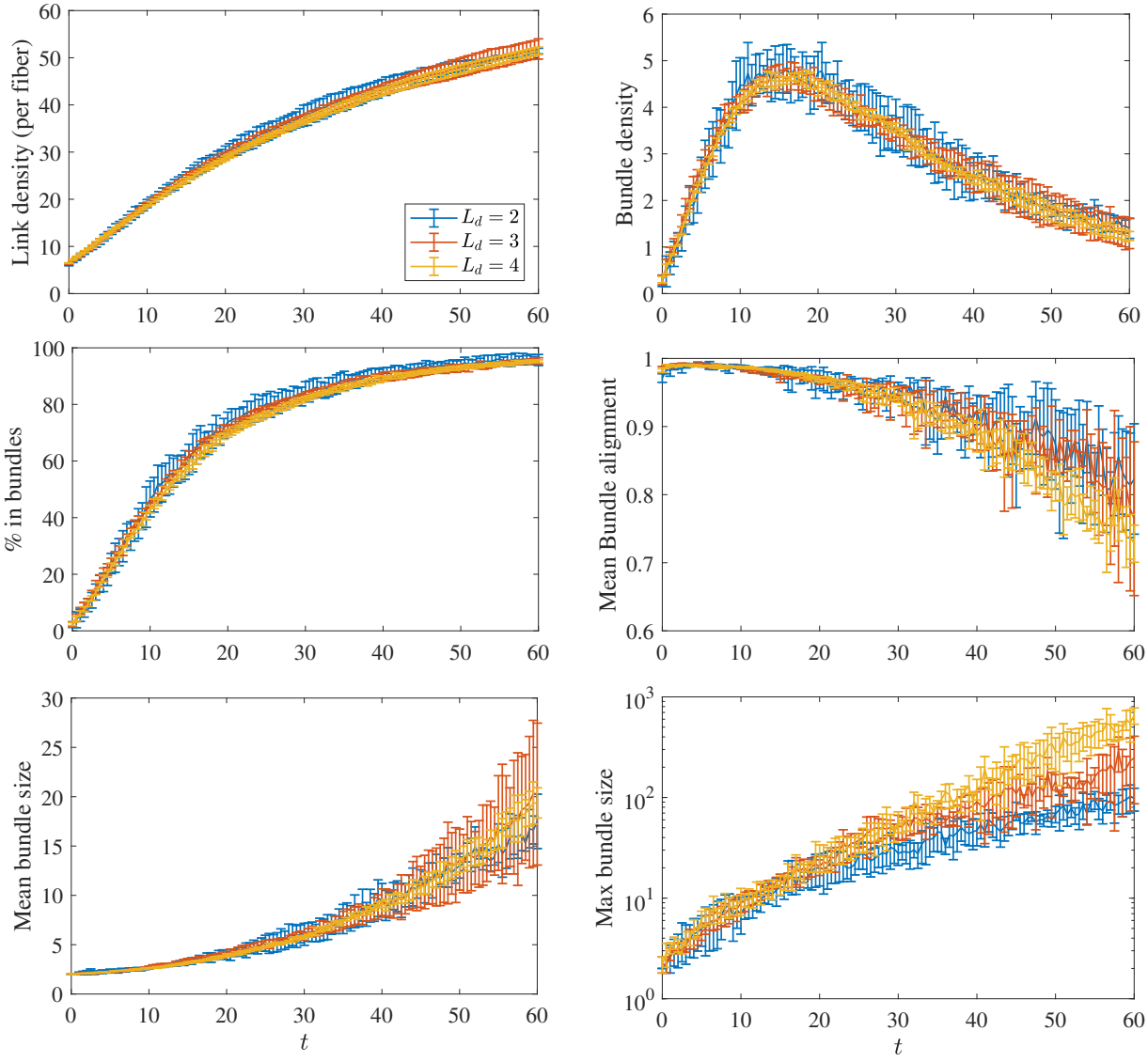

Figure S2: Link density, bundle density, % of fibers in bundles, mean bundle alignment, mean bundle size, and maximum bundle size, in a network of semiflexible ($\kappa = 0.07$ pN·μm^2) non-Brownian filaments with initial mesh size $\ell_m = 0.2$ μm. We show curves with different domain sizes (in μm) to establish that the statistics are repeatable in larger systems. The only statistic which is not repeatable is the maximum bundle size after many of the filaments have collapsed into one bundle ($t \gtrsim 40$ s).

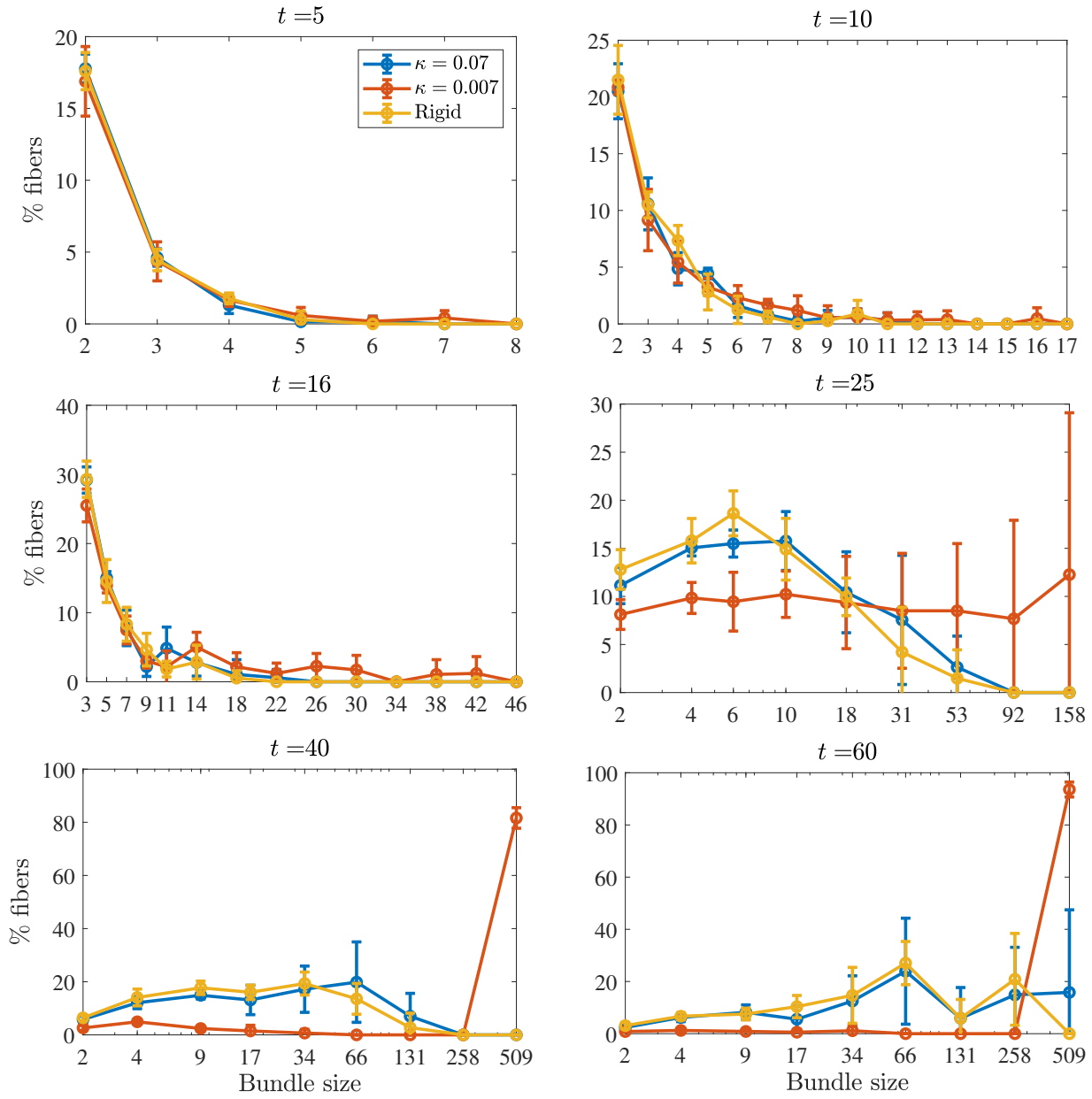

Figure S3: Bundle sizes over time in the system with $F = 675$ semiflexible filaments in a domain of size $L_d = 3$ μm ($\tau_c \approx 16$). We show the percentage of fibers that are in bundles of various sizes over time for $\kappa = 0.07$ pN$\cdot\,\mu$m^2 (blue), $\kappa = 0.007$ pN$\cdot\,\mu$m^2 (orange), and rigid fibers (yellow). For times $t = 25, 40$, and 60 seconds, the x coordinate reflects the center of a histogram bin with logarithmically-scaled width. At $t = 5$ s, 25% of the filaments are in bundles of sizes 2 or 3, while most of the other fibers are not in bundles. At $t = \tau_c = 16$ s, about 50% of the fibers are in bundles of size 10 or less, with a small percentage in larger bundles, and the rest not in bundles at all (this is the composite bundle state). For semiflexible fibers with $\kappa = 0.07$ and rigid fibers, about 75% of the fibers are in bundles of size 30 or larger by $t = 60$, while for fibers with $\kappa = 0.007$ the entire suspension has coalesced together by $t = 40$ seconds.

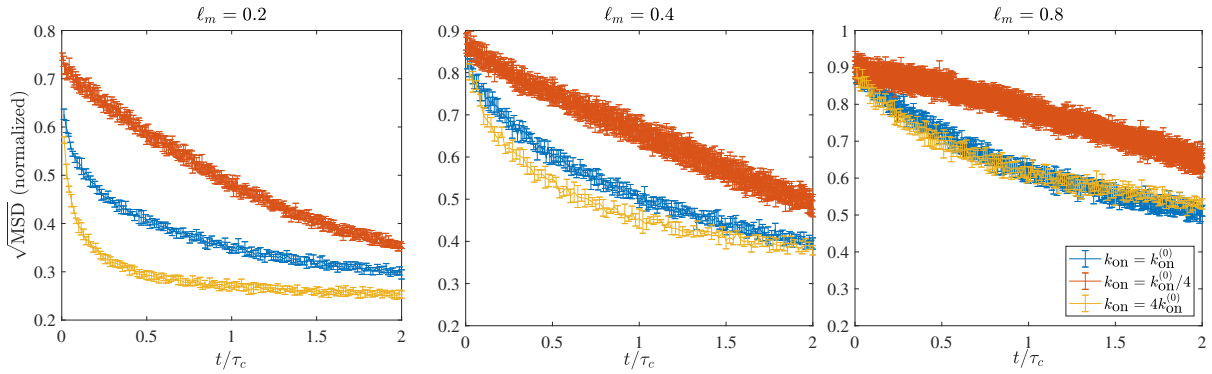

Figure S4: Square root of average mean square displacement of the fibers' centers over a time span of 0.05 seconds for simulations with Brownian dynamics and varying k_{on} (colors) and mesh size (from small mesh size to large going from left to right), all normalized by the value for a freely diffusing fiber. We normalize time by τ_c. While all of the curves show significant decay on the timescale τ_c, it is clear that τ_c is not the only timescale in the problem, since curves with small k_{on} are qualitatively different. This is not a surprise, since we saw in the main text that the bundling process with small k_{on} is more biased towards large bundles (see Fig. 5).

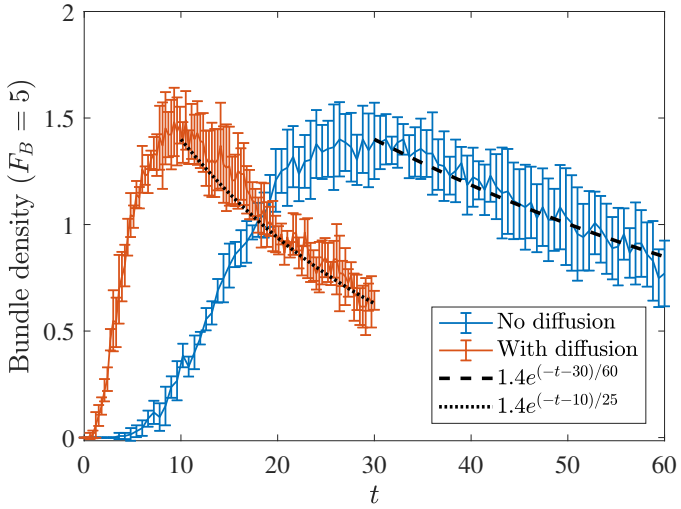

Figure S5: Comparing Brownian and non-Brownian filaments with a minimum of $F_B = 5$ filaments per bundle. In Fig. 3 in the main text, we used a definition of a bundle as having at least two filaments to conclude that Brownian motion accelerates the bundling process by more in the initial stages (factor of about 4) than in the latter (factor of about 2). When we increase to $F_B = 5$ filaments per bundle, we observe the same characteristic growth and decay as with $F_B = 2$, with the peak occurring three-fold faster in simulations with Brownian dynamics and the later dynamics being accelerated by a factor of about two (from a timescale of 60 s to 25 s). These confirm the qualitative (and quantitative) conclusions from Fig. 3 that we made in the main text.

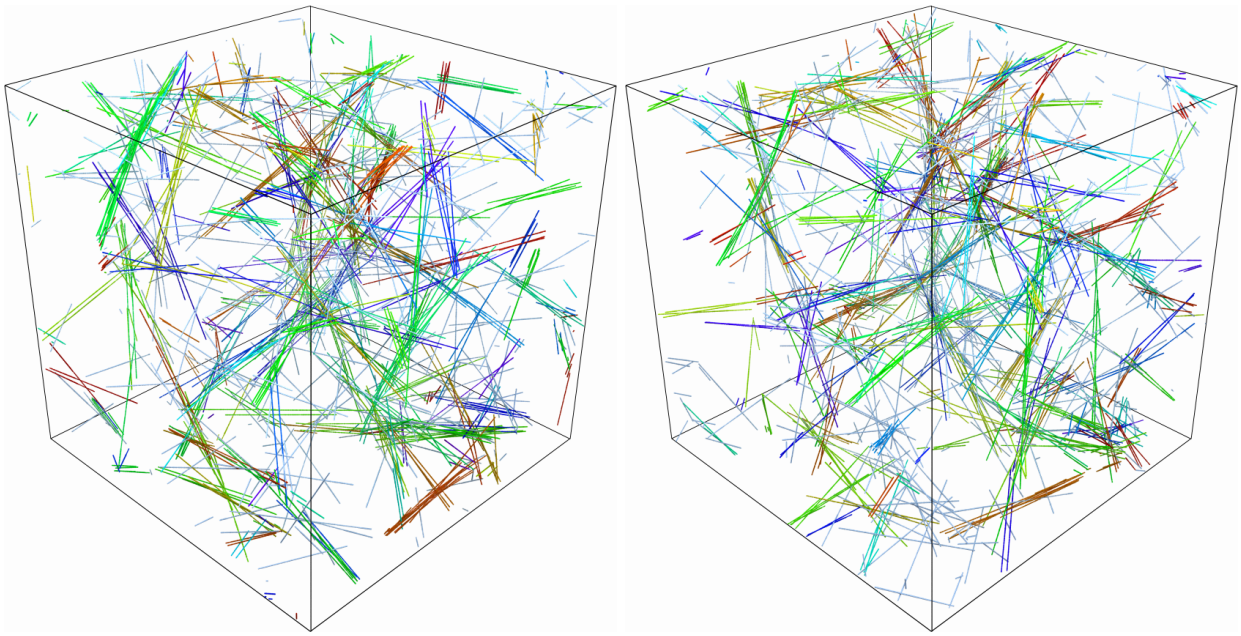

Figure S6: Representative snapshots of a network of rigid fibers without (left) and with (right) Brownian motion. Both snapshots are taken at $t = \tau_c$, which is 16 seconds for simulations without fluctuations and 4 seconds for simulations with fluctuations. The networks are qualitatively the same.

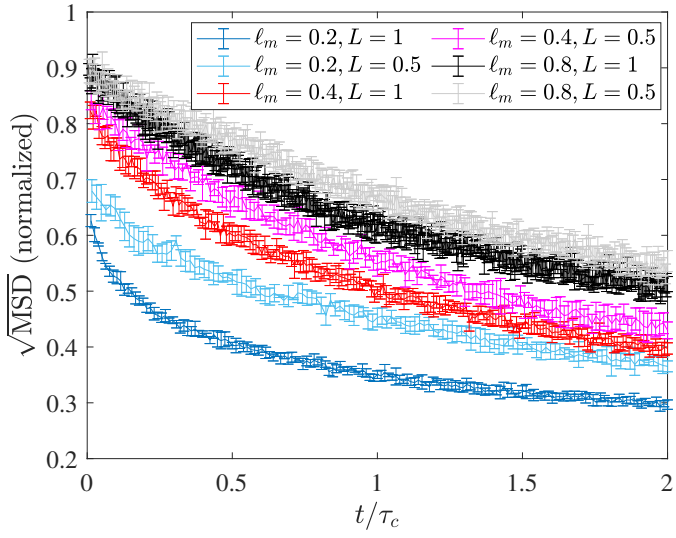

Figure S7: Decay of fibers' centers' displacement for different fiber lengths and mesh sizes. We show (the square root of) the average MSD of the fibers' centers over a time span of 0.05 seconds, normalized by the free space diffusion for fibers of the same length. We show mesh size $\ell_m = 0.2$ μm (blue), 0.4 μm (red), and 0.8 μm (black). Lighter colors are for filament length $L = 0.5$ μm, darker are $L = 1$ μm.

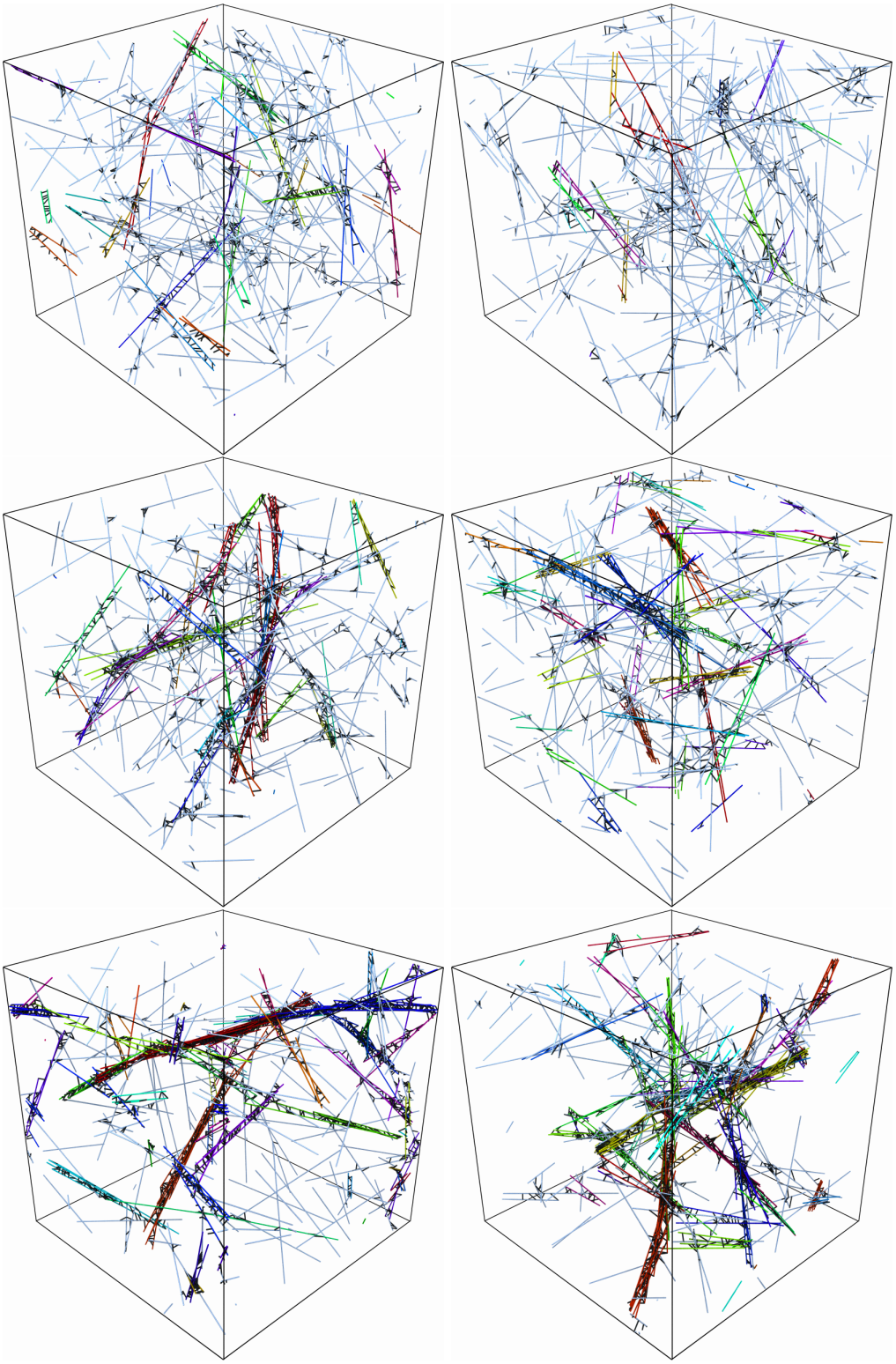

Figure S8: Steady states with fiber turnover for (top to bottom) $\tau_f = \tau_c/2$, $\tau_f = \tau_c$, and $\tau_f = 2\tau_c$ for a system with $L_d = 2$ and $\ell_m = 0.2$. The left column is for non-Brownian fibers ($\tau_c = 16$ seconds) and the right column is for Brownian ones ($\tau_c = 4$ seconds). There is little qualitative difference between the left and right columns, which indicates that the network morphology is controlled primarily by the ratio τ_f/τ_c.